

Quantum Radiometric Calibration

Leif Albers,¹ Jan-Malte Michaelsen,¹ and Roman Schnabel^{1,*}

¹*Institut für Quantenphysik und Zentrum für Optische Quantentechnologien
Universität Hamburg, Luruper Chaussee 149, 22761 Hamburg, Germany*

(Dated: 6 February 2026)

Optical quantum computing, as well as quantum communication and sensing technology based on quantum correlations are in preparation. These require photodiodes for the detection of about 10^{16} photons per second with close to perfect quantum efficiency. Already the radiometric calibration is a challenge. Here, we provide the theoretical description of the quantum radiometric calibration method. Its foundation is squeezed light and Heisenberg's uncertainty principle, making it an example of quantum metrology based on quantum correlations. Unlike all existing radiometric calibration methods, ours is in situ and provides both the detection efficiency and the more stringent quantum efficiency directly for the measurement frequencies of the user application. We calibrate a pair of the most efficient commercially available photodiode at 1550 nm to a system detection efficiency of $(97.20 \pm 0.37)\%$ using 10-dB-squeezed vacuum states. Our method has great potential for significantly higher precision and accuracy, but even with this measurement, we can clearly say that the available photodiode efficiencies for 1550 nm are unexpectedly low, too low for future gravitational wave detectors and for optical quantum computing.

The most commonly used photoelectric sensors include photodiodes that are operated in the unity-gain regime. The ideal case of perfect detection efficiency ($\eta_{DE} = 1$) means that each photon is converted into exactly one photoelectron. A user application also requires negligible dark current. We take this aspect into account through the more strictly defined ‘quantum efficiency’ ($\eta_{QE} \leq \eta_{DE} \leq 1$). With close to perfect quantum efficiency, the photon statistics of light can be mapped one-to-one into photoelectron statistics for high photon fluxes in the range of $10^{15} - 10^{17}/\text{s}$ (without single-photon resolution). Two identical such photodiodes together with a balanced beam splitter and a local oscillator beam of the aforementioned photon flux form a so-called balanced homodyne detector (BHD), which is arguably the most important photoelectric detector in optical quantum technologies. A BHD is able to measure the information of an arbitrarily weak quantum state effectively and completely (‘tomographically’). This includes the zero-point fluctuations of the ground state of an optical mode, which contains *zero* photons. BHDs have been used to realise quantum teleportation [1, 2] and to produce Schrödinger cat states [3, 4]. And they are to be used to read out the optical quantum computer [5–8]. For this, photodiodes with a quantum efficiency close to one ($> 99\%$) are required to properly assign qubits to the light field and to achieve the necessary fault tolerance in the future [8]. To determine the absolute efficiency of photodiodes (detection efficiency, quantum efficiency likewise), national metrology institutes use several calibration steps usually starting with an electrically calibrated cryogenic radiometer [9]. This is used to calibrate a secondary standard, which is either a photo-electric trap detector [10] or a sphere detector [11]. Recently, pyroelectric detectors were tested as secondary standards [12] and an ab-

solute efficiency calibration with a total combined standard deviation of $< 0.28\%$ for wavelengths above $1\text{ }\mu\text{m}$ was achieved.

An entirely different calibration method was presented in [13]. It solely utilises squeezed states of light, the Heisenberg uncertainty principle, and relative photon loss measurements. The detection efficiencies of the presumably best photo diodes on the market for 1064 nm and 1550 nm were calibrated to $(99.5 \pm 0.5)\%$ [13] and $(98.5 \pm 0.7)\%$ [14], respectively, using 15-dB and 13.5-dB squeezed vacuum states of light. (In both experiments, a mirror was used to incorporate the 0.5% reflected light from the photodiode during calibration.) The method should be suitable for calibrating photodiodes as primary standards, however, the theoretical description of the quality of the calibration signal is still missing. Furthermore, there is currently no precise measurement method for the photon escape efficiency of the squeezing resonator, which represents a potential source of significant systematic error. In this work, we present the theoretical description of the calibration signal of quantum radiometric calibration (QRC) as well as the required concept for the measurement of the escape efficiency. We apply the concept *in situ* and determine the escape efficiency of our squeezing resonator to $(98.583 \pm 0.015)\%$. We use “only” 10-dB squeezed vacuum states, but were nonetheless able to precisely determine the efficiency of the presumably most sensitive photodiodes on the market at 1550 nm (from the same manufacturer as calibrated in [14]) to $\eta_{DE} = (97.20 \pm 0.37)\%$ and $\eta_{QE} = (96.9 \pm 0.4)\%$. Implementing retro-reflection increase the values by 0.46%. The value is unexpectedly low and not sufficient for optical quantum computing.

We use the following definitions of the detection efficiency η_{DE} and the quantum efficiency η_{QE} .

$$\eta_{DE} = \frac{U_{\text{tot}} - U_{\text{dark}}}{U_{\text{perf}}}, \quad \eta_{QE} = \frac{U_{\text{tot}} - U_{\text{dark}}}{U_{\text{perf}} + U_{\text{dark}}}, \quad (1)$$

* roman.schnabel@uni-hamburg.de

where the voltages U are transimpedance amplified photo currents measured on continuous-wave light. U_{tot} is the total measurement voltage and U_{dark} is the contribution without light. U_{perf} represents the perfect case, i.e., the unknown voltage that the measurement system would provide if every photon would be converted into exactly one photo electron, combined with zero dark current. In the limit of negligible dark noise, η_{QE} approaches η_{DE} . The challenge is to determine accurately η_{DE} and thus η_{QE} , i.e., to calibrate a photodetector.

The basis of QRC is the measurement of the Heisenberg uncertainty product of the two orthogonal electric field quadratures \hat{X} and \hat{Y} of a (strongly) squeezed vacuum state using a BHD with a pair of photodiodes that are to be calibrated. The result is compared with the inferred uncertainty product of the squeezed state without any decoherence, which we call the ‘Heisenberg reference’. Squeezed states were first described in the early 1970s [15–20], first experimentally realised in the mid 1980s [21–24], and became a user application in 2011 for the first time when they improved the sensitivity of the GEO600 gravitational wave detector in a joint search for gravitational waves together with Virgo [25, 26].

The quantum uncertainties of a squeezed state are Gaussian, and the variances of their extrema ($\Delta^2\hat{X}$ and $\Delta^2\hat{Y}$) obey a Heisenberg uncertainty relation [27–30]. The normalization to the variance of the ground state uncertainty yields

$$\Delta^2\hat{X} \cdot \Delta^2\hat{Y} \geq 1. \quad (2)$$

The lower bound is reached if the squeezed state is pure. The crucial fact is that the uncertainty product of a squeezed vacuum state increases successively with each lost photon, which is illustrated in Fig. 1. Using the setup’s total photon efficiency η , initial squeezed and anti-squeezed quadrature variances $\Delta^2\hat{X}'$ and $\Delta^2\hat{Y}' = 1/\Delta^2\hat{X}'$ change accordingly to [20]

$$\Delta^2\hat{X} = \eta \Delta^2\hat{X}' + (1 - \eta), \quad \Delta^2\hat{Y} = \eta \Delta^2\hat{Y}' + (1 - \eta). \quad (3)$$

The variances on the left sides above can be precisely measured with the BHD allowing for the remaining two unknown quantities η and $\Delta^2\hat{X}' = 1/\Delta^2\hat{Y}'$ to be calculated. $\Delta^2\hat{X}'$ represents the squeeze factor of the produced state inferred for zero decoherence. Removing this quantity from Eqs. (3) yields

$$\eta = \frac{\Delta^2\hat{X} + \Delta^2\hat{Y} - 1 - \Delta^2\hat{X}\Delta^2\hat{Y}}{\Delta^2\hat{X} + \Delta^2\hat{Y} - 2}. \quad (4)$$

The following equation splits the setup’s imperfect total efficiency η in its contributions containing the wanted detection efficiency η_{DE} .

$$\eta = \eta_{\text{esc}} \eta_{\text{prop}} \eta_{\text{mm}} \eta_{\text{DE}}. \quad (5)$$

Accordingly, η_{DE} is found when η and the other three efficiencies are measured. η_{esc} is the photon escape efficiency

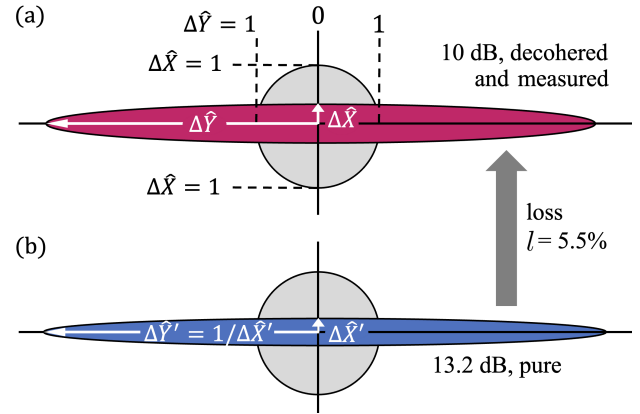


FIG. 1. **Decoherence due to imperfect efficiency** — The ellipses represent the product of the standard deviations $\Delta\hat{X}$ and $\Delta\hat{Y}$ of squeezed states. The circle refers to the ground state (of the same optical mode). (a) Representation of the squeezed state measured in this work with imperfect total setup efficiency η . (b) Representation of the same squeezed state as inferred for perfect efficiency (zero optical loss). The inference corrects for the imperfect efficiency of $\eta = 94.5\%$ (photon loss of 5.5%) according to Eq. (3) yielding a higher squeeze factor and a decreased uncertainty area being at the lower bound of the Heisenberg uncertainty relation in Eq. (2).

from the squeezing resonator, η_{prop} the propagation efficiency from the same resonator to the measurement, and η_{mm} the mode matching efficiency, which corresponds to the square of the interference visibility at the BHD beam splitter. All measurements are photoelectric in nature and take place in situ, i.e., in the same laser-optical QRC setup. This results in low systematic errors and high accuracy. The squeezing resonator’s photon escape efficiency η_{esc} could previously not be measured but just estimated and turned out to be the by far largest error contribution of the method [13]. The concept for measuring η_{esc} is a result of this work and will be discussed later.

We first discuss the measurement principle of η . Its precision increases with an increasing absolute value of the derivative of the measured uncertainty product to η . The measured uncertainty product is according to Eq. (3)

$$\begin{aligned} \Delta^2\hat{X} \cdot \Delta^2\hat{Y} &= [\eta \Delta^2\hat{X}' + (1 - \eta)] \cdot [\eta \Delta^2\hat{Y}' + (1 - \eta)] \\ &= 1 + 4(\eta - \eta^2) \left[\frac{1}{4}(\Delta^2\hat{X}' + \Delta^2\hat{Y}') - \frac{1}{2} \right] \\ &= 1 + 4(\eta - \eta^2)\langle \hat{n} \rangle, \end{aligned} \quad (6)$$

where $(\Delta^2\hat{X}' + \Delta^2\hat{Y}')/4 - 0.5 = \langle \hat{n} \rangle$ is the expectation value for the number of quantum correlated photons of the ‘Heisenberg reference’ [20]. For the pure 13.2-dB squeezed state in Fig. 1(b) $\langle \hat{n} \rangle \approx 4.7$.

We introduce the ‘precision scaling’ of QRC $|S_P|$, which includes the derivative of Eq. (6) to η and the fact that the measurement precisions of $\Delta^2\hat{X}$ and $\Delta^2\hat{Y}$ are

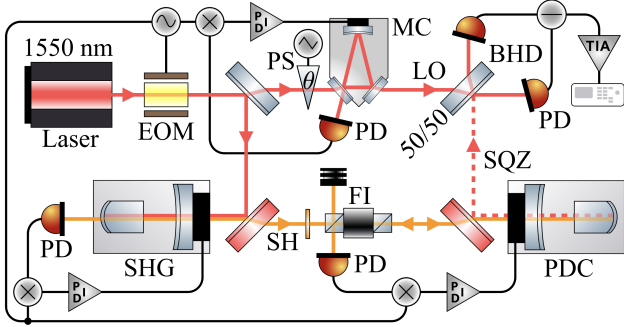


FIG. 2. **Schematic of the QRC setup** — 0.1 W of the output power of a 1550 nm fibre laser was converted into a 775 nm laser beam by resonator-enhanced second harmonic generation (SHG). This light was used to pump our parametric down-conversion (PDC) resonator to generate squeezed vacuum states (SQZ). Two identical photodiodes (PD) to be calibrated were used for the BHD with transimpedance amplifier (TIA). The local oscillator (LO) for the BHD of about 20 mW came from the same fibre laser. The BHD measured the electric field strength of the squeezed states, while the differential phase θ was continuously driven with a phase shifter (PS). The PS was placed in front of a spatial mode cleaner (MC) to avoid beam jitter on the PDs. EOM: electro-optical modulator for Pound-Drever-Hall locking of the length of the MC and SHG resonators, FI: Faraday isolator to avoid self-interference of the second harmonic (SH) light, here 775 nm, PID: proportional-integral-derivative controller.

both proportional to the total efficiency η .

$$|S_P| = \eta^2 \left| \frac{d(1 + 4(\eta - \eta^2)\langle \hat{n} \rangle)}{d\eta} \right| = \eta^2 |4 - 8\eta| \langle \hat{n} \rangle. \quad (7)$$

Thus, the QRC precision increases with $\langle \hat{n} \rangle$ (whereby a limit is set by the fact that the decoherence due to phase fluctuations must remain negligible, see ‘end matter’).

We applied our QRC to a pair of 1550-nm HQE photodiodes from *Laser Components* (with removed protection windows), which were optimized for s-polarized continuous-wave laser light at 1550 nm under 20° angle of incidence. Their semiconductor surfaces were free of dust particles. The two photodiodes formed a balanced homodyne detector for measuring $\Delta^2\hat{X}$ and $\Delta^2\hat{Y}$ of a squeezed state for the determination of η according to Eq. (4). These measurements are not performed at direct current, but at a sideband frequency (within the squeezing bandwidth) for which the photodiodes are designated. Here, we chose 5 MHz. We used resonator-enhanced degenerate parametric down-conversion (PDC) in a second-order non-linear crystal for squeezed light generation [13, 22–24, 31]. A schematic is shown in Fig. 2. The crystals in the SHG and squeezing resonators were periodically poled potassium titanyl phosphate (PPKTP). The crystal geometry was plane-convex and formed a half-monolithic resonator together with a coupling mirror. The crystal was coated to be highly reflective on the convex side and anti-reflective on the other for 1550 nm and 775 nm. The coupling mirror had a design reflectivity of

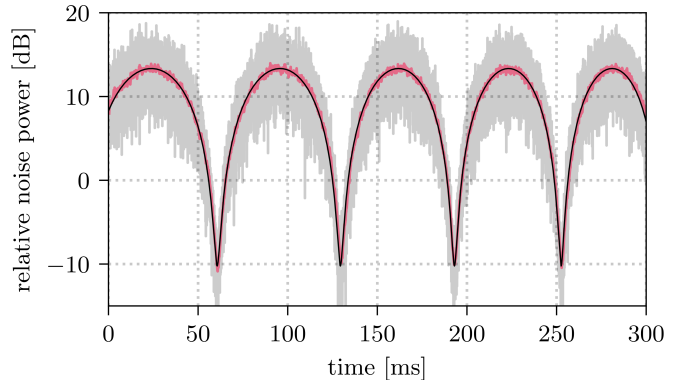


FIG. 3. **Measurement of the uncertainty product** — The voltage from the BHD was converted to a zero-span noise power at 5 MHz with 300 kHz resolution bandwidth using a spectrum analyzer. The traces shown are normalized to the noise power of the optical mode’s ground state. The BHD’s readout phase θ was continuously swept by applying a saw tooth voltage to a piezo electric element behind a steering mirror in the beam path (PS in Fig. 2). The lowest noise power corresponds to $\Delta^2\hat{X}$, the highest to $\Delta^2\hat{Y}$. Per sweep (gray), 32,001 data points were recorded. The red trace corresponds to the same data but 500 Hz low-pass filter on linear scale. The black line shows a model fit, which determined for this single measurement $\Delta^2\hat{X} \approx 0.10$ and $\Delta^2\hat{Y} \approx 19.7$.

$\approx 83\%$ for 1550 nm and $\approx 97.5\%$ for 775 nm light. The temperature profile of the crystal [32–34] was stabilized to provide double-resonance as well as good phase matching. The length of the squeezing resonator was stabilized using the Pound-Drever-Hall (PDH) technique [35]. The squeezed vacuum states at 1550 nm (without any carrier light) ‘escaped’ the squeezing resonator through the coupling mirror, were separated from the 775 nm light via a dichroic mirror, and superimposed with the local oscillator on the BHD’s beam splitter. We directly measured a 10-dB squeezed photon shot noise for a 775-nm pump power of slightly less than 11 mW. The anti-squeezing was close to 13 dB. Increasing the pump power increased the squeeze factor just marginally, while the anti-squeezing increased significantly. We used this measurement to estimate the root mean square (rms) phase noise [36] to $\Delta\theta < (2 \pm 1)$ mrad, which was negligible for the QRC result reported further down.

Fig. 3 shows the measurement of $\Delta^2\hat{X}$ (minima) and $\Delta^2\hat{Y}$ (maxima) for determining the *total efficiency* η . Here, we repeatedly swept the BHD read-out phase θ . This approach offers a few advantages over the alternative of locking the read-out phase to each individual quadrature as used before [13, 14]. First of all, it reduces the complexity of the setup by omitting the stabilization of one degree of freedom. Additionally, slow drifts in the local oscillator and pump power can be neglected. Scanning the read-out phase also guarantees that there is no systematic error in the locking point and ensures that each quadrature is optimally measured at some point. The traces in Fig. 3 already include dark noise subtraction and

normalisation to the ground state variance. The variance of the ground state was measured with the signal input of the BHD blocked. The variance of the dark noise was measured with all light fields blocked.

The traces in Fig. 3 were fitted with the model

$$\Delta^2 X(\varphi(t)) = \Delta^2 X_{\text{sqz}} \cos(\varphi(t))^2 + \Delta^2 X_{\text{asqz}} \sin(\varphi(t))^2 \quad (8)$$

$$\varphi(t) = \varphi_0 + \varphi_1 t + \varphi_2 t^2, \quad (9)$$

where the phase evolution of the figures x-axis was given by the piezo expansion and fitted as given in Eq. (9). Fig. 3 shows one of altogether 100 measurements. Every measurement provided an efficiency value η using Eq. (4). The statistics provided $\eta = (94.48 \pm 0.22)\%$. For the 20° angle of incidence used, $(0.46 \pm 0.06)\%$ of the light was reflected from the photo diodes. A retro-reflector would have increased the values of η , η_{DE} , and η_{QE} accordingly. Most likely, our error specification would have *decreased* minimally, see Eq. (7).

The *escape efficiency* η_{esc} of the squeezing resonator could previously only be estimated using an absorption value of the crystal material from the literature [37] and rather uncertain crystal and coupling mirror coating specifications from the manufacturer [13]. Furthermore, potential surface inhomogeneities and small dust particles in the squeezing resonator, which make the value of η_{esc} dependent on its alignment, could not be taken into account. In [13], the inaccuracy in the determination of η_{esc} clearly dominated the calibration error.

The escape efficiency of the quantum correlated photons from the squeezing resonator is given by

$$\eta_{\text{esc}} = \frac{1 - r^2}{1 - r^2 + \ell_{\text{rt}}^2}, \quad (10)$$

where r^2 is the reflectivity of the ramped coupling mirror in Fig. 4 and ℓ_{rt}^2 is the cavity's relative photon loss per roundtrip, with contributions ℓ_{scat}^2 , ℓ_{abs}^2 , ℓ_{trans}^2 , and ℓ_{refl}^2 .

Our ‘in-situ’-method solved aforementioned inadequacy by determining r^2 and ℓ_{rt}^2 on the finally aligned squeezing resonator, thus including potential local scattering and absorbing defects. We first mode-matched a dim auxiliary 1550-nm field into the squeezing resonator from its over-coupled side. The retro-reflected beam was monitored by a photodiode while the resonator length was scanned with a piezoelectric element and external 775-nm light blocked. A second PD (which was insensitive to 1550 nm light) simultaneously confirmed that no second harmonic light was produced. To achieve this, the temperature of the crystal was set to a conversion minimum under strong pumping. The light power reflected from the scanned resonator reads

$$I(\varphi(t)) = \left| \frac{r - \sqrt{1 - \ell_{\text{rt}}^2} e^{-2i\varphi(t)}}{1 - r\sqrt{1 - \ell_{\text{rt}}^2} e^{-2i\varphi(t)}} \right|^2 I_0, \quad (11)$$

where I_0 is the intensity of the incident beam. Fitting Eq. (11) to the measured light power unambiguously provided the quantities in Eq. (10) and thus η_{esc} .

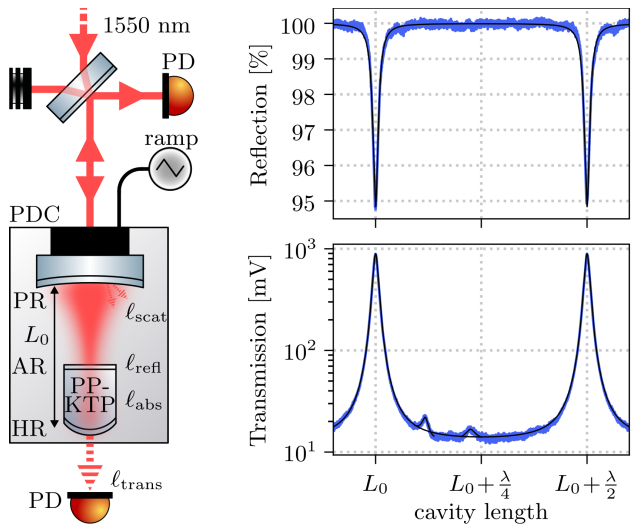


FIG. 4. **Determining the escape efficiency** — Left: Squeezing resonator whose escape efficiency η_{esc} needs to be determined in a separate measurement. η_{esc} is imperfect due to intra-cavity photon scattering (ℓ_{scat}^2) and absorption (ℓ_{abs}^2) at all three intra-cavity surfaces and during crystal transmission. Further photon losses are the residual transmission (ℓ_{trans}^2) and reflection (ℓ_{refl}^2) of the convex and plane crystal surfaces, respectively. Exactly the same loss sources also reduce the reflectivity of the resonator according to Eq. (11), which is accessible through an in-situ measurement of mode-matched, retro-reflected light. AR, PR, HR: anti-, partial, and high-reflectivity coating. Top right: Measurement of the retro-reflected light while the resonator's length is scanned. Dips occur on resonance when the light couples and experiences the intra-cavity loss (to be up-scaled by the imperfect mode matching). The black line in the measurement graph is the theoretical model with fitted coupling mirror reflectivity and roundtrip loss. Bottom right: Simultaneous measurement of transmitted light provides the imperfect mode matching.

Fig. 4 shows our setup for determining η_{esc} (left), a measurement graph of the reflected light power (top right), and the simultaneously measured transmitted power (bottom right). The latter provided a cavity mode matching value of $(98.58 \pm 0.23)\%$ (main peak divided by sum of all peaks), which was required to scale up the loss dip in the top right graph. The fit of Eq. (11) to the up-scaled top right graph required a simultaneous fit of the scanning speed, which we approximated by $\varphi(t) = \varphi_0 + \varphi_1 t + \varphi_2 t^2$. Our in-situ measurement yielded $r^2 = (82.79 \pm 0.35)\%$ and $\ell_{\text{rt}}^2 = (0.247 \pm 0.007)\%$ and thus $\eta_{\text{esc}} = (98.583 \pm 0.015)\%$ according to Eq. (10).

The *propagation efficiency* η_{prop} and the *mode matching efficiency* η_{mm} were measured in the established manner, which is described in the ‘end matter’ to this letter. The measurements yielded $\eta_{\text{prop}} = (99.49 \pm 0.25)\%$ and $\eta_{\text{mm}} = v^2 = (99.11 \pm 0.17)\%$.

The two photodiodes that were calibrated in this work

have an average detection efficiency for 1550 nm light of

$$\begin{aligned}\eta_{DE} &= \frac{(94.48 \pm 0.22)\% / (98.583 \pm 0.015)\%}{(99.49 \pm 0.25)\% \times (99.11 \pm 0.17)\%} \\ &= (97.20 \pm 0.37)\%.\end{aligned}\quad (12)$$

Our error bar corresponds to the total combined standard deviation. It is dominated by statistical errors in the individual measurements and can be further reduced by increasing the measurement time, using lower-loss optics and also fewer optics for beam guidance and focusing on the photodiodes. Already with this experiment we almost achieve the combined standard deviation reported in Ref.[12]. Unlike [12], we exclusively use the photoelectric effect and not the pyroelectric effect, for which light must heat a material through absorption.

The quantum efficiency is derived from the detection efficiency, taking into account the measured dark noise at 5 MHz, see Eq.(1). For the local oscillator power of 10 mW used, we obtain the only slightly lower value of $\eta_{QE}(10 \text{ mW}, 5 \text{ MHz}) = (96.9 \pm 0.4)\%$. We note that in our previous work [13], we only specified the value for detection efficiency according to Eq.(1).

In conclusion, we calibrated the presumably best photodiodes for 1550 nm on the market (*Laser Components*) to a detection efficiency of just $(97.20 \pm 0.37)\%$. This value is insufficient for optical quantum computers

based on the continuous variables X and Y [5–8] and for the current design of the low-frequency detector of the Einstein Telescope (ET), which is intended to exploit 10-dB squeezed light at 1550 nm. The ball is now in the manufacturers' court.

The QRC method presented in detail and used here has several unique features compared to established methods. It uses only Heisenberg's uncertainty principle and the photoelectric effect. Noise powers at the relevant measurement frequency are used for calibration. QRC is thus suitable for determining quantum efficiencies that depend on the measurement frequency. We have shown that absolute calibration with an uncertainty of only 0.37% is possible with squeezed vacuum states in the achievable 10 dB range. Squeeze lasers of this quality are commercially available [38]. The QRC method represents an important tool for the realisation of fault-tolerant optical CV quantum computers.

This work was supported and partly financed (L.A.) by the DFG under Germany's Excellence Strategy EXC 2121 "Quantum Universe" – 390833306.

L.A. performed the final experiments and the data analysis. J.-M.M. performed initial η_{esc} -measurements. R.S. invented QRC and the η_{esc} -measurement approach, developed the theoretical QRC description, and prepared the manuscript with the help of L.A.

[1] A. Furusawa, J. L. Sørensen, S. L. Braunstein, C. A. Fuchs, H. J. Kimble, and E. S. Polzik. Unconditional quantum teleportation. *Science*, 282(5389):706–9, oct 1998.

[2] W. P. Bowen, N. Treps, B. C. Buchler, R. Schnabel, T. C. Ralph, H.-A. Bachor, T. Symul, and P. K. Lam. Experimental investigation of continuous-variable quantum teleportation. *Physical Review A*, 67(3):032302, mar 2003.

[3] A. Ourjoumtsev, R. Tualle-Brouri, J. Laurat, and P. Grangier. Generating Optical Schrödinger Kittens for Quantum Information Processing. *Science*, 312(5770):83–86, apr 2006.

[4] J. S. Neergaard-Nielsen, B. Melholt Nielsen, C. Hettich, K. Mølmer, and E.S. Polzik. Generation of a superposition of odd photon number states for quantum information networks. *Physical Review Letters*, 97(8):5, aug 2006.

[5] M. V. Larsen, X. Guo, C. R. Breum, J. S. Neergaard-Nielsen, and U. L. Andersen. Deterministic generation of a two-dimensional cluster state. *Science*, 366(6463):369–372, oct 2019.

[6] Kosuke Fukui and Shuntaro Takeda. Building a large-scale quantum computer with continuous-variable optical technologies. *Journal of Physics B: Atomic, Molecular and Optical Physics*, 55(1):012001, jan 2022.

[7] S. Konno, W. Asavanant, F. Hanamura, H. Nagayoshi, K. Fukui, A. Sakaguchi, R. Ide, F. China, M. Yabuno, S. Miki, H. Terai, K. Takase, M. Endo, P. Marek, R. Filip, P. van Loock, and A. Furusawa. Logical states for fault-tolerant quantum computation with propagating light. *Science*, 383(6680):289–293, jan 2024.

[8] M. V. Larsen, J. E. Bourassa, S. Kocsis, J. F. Tasker, R. S. Chadwick, C. González-Arciniegas, J. Hastrup, C. E. Lopetegui-González, F. M. Miatto, A. Motamed, R. Noro, G. Roeland, R. Baby, H. Chen, P. Contu, I. Di Luch, C. Drago, M. Giesbrecht, T. Grainge, I. Krasnokutska, M. Menotti, B. Morrison, C. Puviraj, K. Rezaei Shad, B. Hussain, J. McMahon, J. E. Ortmann, M. J. Collins, C. Ma, D. S. Phillips, M. Seymour, Q. Y. Tang, B. Yang, Z. Vernon, R. N. Alexander, and D. H. Mahler. Integrated photonic source of Gottesman–Kitaev–Preskill qubits. *Nature*, 642(8068):587–591, jun 2025.

[9] K. D. Stock and H. Hofer. Present state of the PTB primary standard for radiant power based on cryogenic radiometry. *Metrologia*, 30(4):291, 1993.

[10] M. López, H. Hofer, and S. Kück. High accuracy measurement of the absolute spectral responsivity of ge and ingaas trap detectors by direct calibration against an electrically calibrated cryogenic radiometer in the near-infrared. *Metrologia*, 43(6):508, 2006.

[11] George P. Eppeldauer, Howard W. Yoon, Yuqin Zong, Thomas C. Larason, A. Smith, and M. Racz. Radiometer standard for absolute responsivity calibrations from 950 nm to 1650 nm with 0.05% ($k=2$) uncertainty. *Metrologia*, 46(4):S139, 2009.

[12] Brian G. Alberding, John T. Woodward IV, Ping-Shine

Shaw, Leonard M. Hanssen, Catherine C. Cooksey, and Joseph P. Rice. Pyroelectric detector-based method for low uncertainty spectral irradiance and radiance responsivity calibrations in the infrared using tunable lasers. *Applied optics*, 61(11):2957–2966, 2022.

[13] Henning Vahlbruch, Moritz Mehmet, Karsten Danzmann, and Roman Schnabel. Detection of 15 dB squeezed states of light and their application for the absolute calibration of photoelectric quantum efficiency. *Physical Review Letters*, 117(11):110801, 2016.

[14] F. Meylahn, B. Willke, and H. Vahlbruch. Squeezed States of Light for Future Gravitational Wave Detectors at a Wavelength of 1550 nm. *Physical Review Letters*, 129(12):121103, sep 2022.

[15] David Stoler. Equivalence Classes of Minimum Uncertainty Packets. *Physical Review D*, 1(12):3217–3219, jun 1970.

[16] E. Y. C. Lu. New coherent states of the electromagnetic field. *Lettere Al Nuovo Cimento Series 2*, 2(24):1241–1244, dec 1971.

[17] Horace Yuen. Two-photon coherent states of the radiation field. *Physical Review A*, 13(6):2226–2243, jun 1976.

[18] D. F. Walls. Squeezed states of light. *Nature*, 306(5939):141–146, nov 1983.

[19] G. Breitenbach, S. Schiller, and J. Mlynek. Measurement of the quantum states of squeezed light. *Nature*, 387(6632):471–475, may 1997.

[20] Roman Schnabel. Squeezed states of light and their applications in laser interferometers. *Physics Reports*, 684:1–51, apr 2017.

[21] R. E. Slusher, L. W. Hollberg, B. Yurke, J. C. Mertz, and J.F. Valley. Observation of Squeezed States Generated by Four-Wave Mixing in an Optical Cavity. *Physical Review Letters*, 55(22):2409–2412, nov 1985.

[22] Ling-An Wu, H.J. Kimble, J.L. Hall, and Huifa Wu. Generation of squeezed states by parametric down conversion. *Phys. Rev. Lett.*, 57:2520–2523, Nov 1986.

[23] E. S. Polzik, J. Carri, and H. J. Kimble. Spectroscopy with Squeezed Light. *Physical Review Letters*, 68:3020, 1992.

[24] H. Vahlbruch, M. Mehmet, S. Chelkowski, B. Hage, A. Franzen, N. Lastzka, S. Goßler, K. Danzmann, and R. Schnabel. Observation of Squeezed Light with 10-dB Quantum-Noise Reduction. *Physical Review Letters*, 100(3):033602, jan 2008.

[25] J. Abadie *et al.* A gravitational wave observatory operating beyond the quantum shot-noise limit. *Nature Physics*, 7(12):962–965, sep 2011.

[26] H. Grote, K. Danzmann, K.L. Dooley, R. Schnabel, J. Slutsky, and H. Vahlbruch. First Long-Term Application of Squeezed States of Light in a Gravitational-Wave Observatory. *Physical Review Letters*, 110(18):181101, may 2013.

[27] W. Heisenberg. Über den anschaulichen Inhalt der quantentheoretischen Kinematik und Mechanik. *Zeitschrift für Physik*, 43(3-4):172–198, mar 1927.

[28] E. H. Kennard. Zur Quantenmechanik einfacher Bewegungstypen. *Zeitschrift für Physik*, 44(4-5):326–352, apr 1927.

[29] H. Weyl. Quantenmechanik und Gruppentheorie. *Zeitschrift für Physik*, 46(1-2):1–46, nov 1927.

[30] H. P. Robertson. The Uncertainty Principle. *Physical Review*, 34(1):163–164, jul 1929.

[31] Axel Schönbeck, Fabian Thies, and Roman Schnabel. 13 dB squeezed vacuum states at 1550 nm from 12 mW external pump power at 775 nm. *Optics Letters*, 43(1):110, jan 2018.

[32] Nico Lastzka and Roman Schnabel. The Gouy phase shift in nonlinear interactions of waves. *Optics Express*, 15(12):7211–7217, nov 2007.

[33] Axel Schönbeck. *Compact squeezed-light source at 1550 nm*. PhD thesis, University of Hamburg, 2018.

[34] Malte Hagemann, Jascha Zander, Axel Schönbeck, and Roman Schnabel. 10-dB squeeze laser tuneable over half a nanometer around 1550 nm. *Optics Express*, 32(5):7954, 2024.

[35] Ronald W. P. Drever, John L. Hall, Frank V. Kowalski, James Hough, G. M. Ford, A. J. Munley, and Hywel Ward. Laser phase and frequency stabilization using an optical resonator. *Applied Physics B*, 31:97–105, 1983.

[36] T. Aoki, Go Takahashi, and A. Furusawa. Squeezing at 946nm with periodically poled KTiOPO₄. *Optics Express*, 14(15):6930, 2006.

[37] J. Steinlechner, S. Ast, C. Krüger, A. Pal Singh, T. Eberle, V. Händchen, and R. Schnabel. Absorption measurements of periodically poled potassium titanyl phosphate (PPKTP) at 775 nm and 1550 nm. *Sensors (Basel, Switzerland)*, 13(1):565–73, jan 2013.

[38] Noisy Labs GmbH, <https://noisy-labs.com/>.

[39] H. Vahlbruch, S. Chelkowski, K. Danzmann, and R. Schnabel. Quantum engineering of squeezed states for quantum communication and metrology. *New Journal of Physics*, 9(10):371, oct 2007.

[40] A. Franzen, B. Hage, J. DiGuglielmo, J. Fiurášek, and R. Schnabel. Experimental Demonstration of Continuous Variable Purification of Squeezed States. *Physical Review Letters*, 97(15):150505, oct 2006.

[41] M. Mehmet, S. Ast, T. Eberle, S. Steinlechner, H. Vahlbruch, and R. Schnabel. Squeezed light at 1550 nm with a quantum noise reduction of 12.3dB. *Optics Express*, 19(25):25763–72, dec 2011.

END MATTER

Measurement of the propagation efficiency η_{prop} – We blocked the second harmonic pump beam and coupled an auxiliary 1550-nm field through the PDC cavity from the under-coupled side. The transmitted light on cavity resonance was in the same mode as the squeezed vacuum and experienced the same optical losses along the down stream path. Measuring its power behind the coupling mirror P_{cm} and in front of each homodyne photodiode $P_{\text{PD1,PD2}}$ allowed for determining the propagation efficiency $\eta_{\text{prop}} = (P_{\text{PD1}} + P_{\text{PD2}})/P_{\text{cm}}$. The optical loss of the coupling mirror itself was dominated by its anti-reflective coating with AR = 500 ppm \pm 500 ppm. Our measurement yielded $\eta_{\text{prop}} = (99.49 \pm 0.25)\%$.

Measurement of the mode matching efficiency η_{mm} – We used the same auxiliary beam as before, precisely adjusted its power to match that of the LO, and measured the interference contrast at the beam splitter of the BHD. The differential phase θ was swept linearly by a piezo-actuated steering mirror and the resulting fringes were recorded using a single photodiode of the

BHD. The fringe visibility was derived according to $v = (U_{\max} - U_{\min})/(U_{\max} + U_{\min})$, where $U_{\max,\min}$ were the photoelectric voltages after subtraction of the voltage without any light. Our measurement yielded $\eta_{\text{mm}} = v^2 = (99.11 \pm 0.17)\%$.

Balanced homodyne detection – The most important test for ruling out systematic errors caused by the BHD is to verify its proportionality. The measured spectral noise power must be proportional to the LO power across the entire target measurement range when the signal input is blocked, i.e., when the vacuum state is measured (see for instance Fig. 2 in Ref. [39]). If the noise power increases

more rapidly, it is not the noise power of the ground state that is being measured, but that of other noise sources, e.g., scattered photons. If it increases more slowly, this is an indication of saturation of the amplifier electronics. Regardless of the BHD, a systematic error can arise if the phase θ of the squeezed light fluctuates during the measurement [40]. This type of decoherence also leads to a reduction in the squeeze factor, even if all photons are detected. By operating the squeezing resonator close to its oscillation threshold, the phase noise becomes visible and can be quantified (see for instance Figs. 4 in Ref. [41]). Ideally, QRC uses a range of $\langle \hat{n} \rangle$ in which phase fluctuations are demonstrably irrelevant.